Received: 4 September 2018 | Revised: 8 February 2019 | Accepted: 9 February 2019

DOI: 10.1002/sia.6633

SPECIAL ISSUE ARTICLE

WILEY SURFACE and INTERFACE ANALYSIS

EIS investigation of a Ce-based posttreatment step on the corrosion behaviour of Alclad AA2024 anodized in TSA

Oscar Mauricio Prada Ramirez[1] | Fernanda Martins Queiroz[1] | Maysa Terada[2] | Uyime Donatus[3] | Isolda Costa[3] | Marie-Georges Olivier[4,5] | Hercílio Gomes de Melo[1]

[1] Escola Politécnica da Universidade de São Paulo, São Paulo, São Paulo, Brazil

[2] CNPEM/LnNano, Rua Giuseppe Maximo Scolfaro, Centro Nacional de Pesquisa em Energia e Materiais/Laboratório Nacional de Nanotecnologia, Campinas, São Paulo, Brazil

[3] IPEN/CNEN-SP, Instituto de Pesquisas Energéticas e Nucleares / Comissão Nacional de Energia Nuclear, São Paulo, São Paulo, Brazil

[4] Service de Science des Matériaux, Université de Mons, Mons, Belgium

[5] Materia Nova asbl, Mons, Belgium

Correspondence
Oscar Mauricio Prada Ramirez, Escola Politécnica da Universidade de São Paulo, Av. Prof. Mello de Moraes, São Paulo 2463, São Paulo, Brazil.
Email: oscarmprada@usp.br

Funding information
CNPq, Grant/Award Numbers: 168625/2017-2 and 400895/2014-5; FAPESP, Grant/Award Numbers: 2018/01096-5 and 2013/13235-6

In the aircraft industry, anodizing and posttreatment steps use Cr (VI) compounds, which, despite offering good corrosion resistance and self-healing properties, are highly toxic and carcinogenic. Ce compounds are recognized as efficient corrosion inhibitors for Al alloys, and several works report self-healing ability for these chemicals. In this investigation, the corrosion resistance of Alclad AA2024-T3 alloy anodized in tartaric-sulphuric acid (TSA) bath and posttreated in a solution comprising cerium nitrate without and with hydrogen peroxide was evaluated. The purpose is to investigate the potentiality of using hydrothermal treatment in Ce nitrate solution as candidate to replace Cr (VI) posttreatment. The aim is to provide a posttreatment step which, while improving the corrosion resistance, does not plug the mouths of the pores maintaining the adhesion properties of the porous anodic layer. Microstructural characterization was carried out by SEM-EDS whereas corrosion resistance was evaluated by EIS. The surface analysis showed that the posttreatments, all performed at 50°C, kept the open structure of the pores. EIS analysis showed that the posttreatments performed in the H_2O_2 solution for short immersion times were the most effective in improving the corrosion resistance of the samples, whereas electrical equivalent circuit (EEC) fitting of the data indicated sealing of the porous layer during the immersion of the different samples in the test solution. SEM-EDS analysis of the samples posttreated in the H_2O_2 containing solution, prior and after the corrosion test, showed the presence of Ce oxy-hydroxide randomly deposited on the sample surface, indicating that Ce could be incorporated/stored in the anodic layer.

KEYWORDS

aluminium, anodizing, Ce, EIS, posttreatment, TSA

1 | INTRODUCTION

The low density and high tensile strength of aluminium alloys 2024-T3 (AA2024-T3) make them a preferred material in the aerospace industry. The good mechanical properties are achieved by means of a complex microstructure, resulting from the addition of several alloying elements, such as Mg, Mn, and Cu, and thermomechanical treatments performed during the production stage.[1] However, the microstructural complexity of this alloy, with the presence of intermetallics, dispersoids, and strengthening particles,[2-7] considerably reduces its resistance to localized corrosion.[8,9] Thus, for use in aircraft, AA2024-T3 requires an efficient protection system.

One of the most frequently used methodologies to increase the corrosion resistance of Al alloys is anodizing. The procedure consists of thickening the oxide layer by applying an anodic potential to the Al piece immersed in an electrolyte of suitable composition. When

performed in acidic solution, anodizing results in a duplex layer composed of a very thin barrier layer with high resistance to corrosion and a thicker porous layer, whose microstructure is ideal for increasing adhesion between the substrate and protective coatings.[2,10] In the aerospace industry, for more than 60 years, anodizing has been performed in acidic baths containing chromate ions, mainly for structural components.[11] In a bid to increase the corrosion resistance, the anodized alloy is then subjected to the commercial alodine treatment (which also contains chromates) and by the application of a primer (generally containing chromate-base inhibitors) and a topcoat.[8,9] To ensure good adhesion of the primer, the porous layer cannot be sealed.

The extensive use of chromate ions in surface treatments with the aim of increasing the corrosion resistance of metallic substrates is justified by their low cost and the self-healing properties presented by systems containing these ions.[12,13] Zhao et al[14] summarize that the mechanism of corrosion inhibition of Al by chromate ions can be ascribed to the presence of very soluble and high oxidation state chromate ions (CrO_4^{2-} or $Cr_2O_7^{2-}$) within the composition of the protecting system. Upon exposure to electrolytes, these species are dissolved (lixiviated) and migrate to defective sites, wherein they are reduced to highly insoluble Cr (III) oxy-hydroxides (Cr_2O_3 or $Cr(OH)_3$), thus extinguishing the localized corrosion. However, the use of chromate-based surface treatments for corrosion protection of metallic substrates, although consolidated and efficient, is extremely aggressive to human health and the environment,[4] and their use is already being banned in several industrial sectors. Nevertheless, due to high safety requirements, their application is still allowed in the aerospace industry. As a result, currently, several research works have been devoted to investigating the effectiveness of chromium-free surface treatments for corrosion protection of high strength Al alloys.

With specific reference to anodizing, various alternative bath compositions are being employed by commercial aviation. Among them, the anodizing in boric-sulfuric acid patented by Boeing,[15] in tartaric sulfuric acid (TSA) used by Airbus,[16] and in phosphoric and sulfuric acid bath, which, according to Abrahami et al,[11] should be used by Fokker in the near future. The TSA anodizing procedure, used in this study, is considered environmentally friendly and results in anodized layers with corrosion resistance similar to those produced in chromic acid electrolytes.[17] Authors suggest that the improved corrosion resistance could be ascribed either to the retention of tartaric acid derivatives within the pores of the anodized layer, stabilizing the pH and avoiding alkalinization or local acidification associated with corrosion processes,[18] or to the formation of chelates with ionic species of more noble elements present in the alloy composition, which would be dissolved inside the pores during the corrosive process.[19] Regarding the fatigue resistance, another important property that must be looked at when anodizing procedures are employed, data available in the fast magazine, from Airbus, show similar behaviour for samples anodized either in chromic acid or TSA baths.[16]

Typically, anodized pieces are stored prior to their use and coating application.[20] To improve the corrosion protection, the pieces are normally pretreated with Alodine, a commercially available treatment (containing F^- and chromates), before primer application. This treatment introduces chromate ions in the skeleton of the porous layer conferring self-healing properties to the system, which then become able to hinder corrosion activity at defective sites of the coating (primer + topcoat) system during ageing.[17]

Ce conversion coatings have been widely investigated as a methodology for protecting Al alloys from corrosion. In the early studies, it was verified that the addition of few hundred ppm of Ce salts to a NaCl solution produced a conversion layer composed of oxides and hydroxides of Ce (III) and Ce (IV), able to significantly reduce the corrosion rate.[21] However, in these initial studies, the formation and thickening of the Ce-oxide layer from the aqueous solution occurred very slow and could take several days.[21] However, Wilson and Hinton[22] showed that the addition of H_2O_2 to an aqueous solution containing Ce salts caused precipitation of a relatively thick conversion layer on the alloy surface, reducing the treatment time to only a few minutes. With this new perspective, the protection against corrosion of Al alloys by Ce conversion layers began to be investigated by other researchers.[23-27]

Self-healing properties have been attributed to Ce oxide films deposited on Al alloys.[28-30] For instance, in the study performed by Ershov et al,[29] on a clad AA2024 protected with a CeO_2 layer deposited by magnetron sputtering, it was suggested that the increased polarization resistance with immersion time in the test electrolyte (observed for a coating with certain composition—highest amount of oxygen introduced during the sputtering process) could be ascribed to the interaction between the cerium and aluminium oxide layers, leading to the blockage of defective sites. On the other hand, in the investigation carried out by Yoganandan et al,[30] the increased impedance modulus with immersion time and the superior stability of a Zr-Ce conversion coating applied on AA2024-T3 when compared with a Zr-only coating was attributed to the migration of Ce^{3+} species to defective sites at which they would precipitate at cathodic regions as insoluble CeO_2. Using a simulated scratch-cell wherein bare AA2024-T3 was exposed together with a sample protected by the Zr-Ce conversion coating to the same electrolyte, the authors documented increased impedance response of the bare sample with immersion time, which was associated with the precipitation of Ce-oxide at cathodic sites.[30] Finally, several works in the literature report self-healing abilities for different coatings when modified with Ce ions.[31-34]

In the present study, the effect of a posttreatment step consisting of immersion in solutions containing Ce ions on the microstructure and the corrosion resistance of clad AA2024-T3 anodized in TSA was investigated. In addition to improving the corrosion resistance of the system, the treatment aims to create a reservoir of Ce-ions which could impart corrosion inhibiting properties (self-healing) to an anodized layer that, in future investigations, will be further protected by coatings (primer and top coating). Further, aiming for industrial application, which demands adhesion properties of the anodized layer, it is essential that the treatments employed do not plug the pores. Anodizing was carried out in a clad alloy to evaluate more clearly possible changes and damages caused to the anodized layer by the different posttreatments.

It should be noted that, in the literature, there are already studies where posttreatments with Ce ions were used to increase the corrosion resistance of anodized aluminium alloys in TSA.[35-37] However, relatively thick conversion layers have been produced in these studies. Contrary to these previous studies, maintaining the porosity of the anodic layer is an essential aspect of the present investigation, thereby maintaining its adhesion properties.

2 | EXPERIMENTAL

The clad AA2024-T3 sheet, with nominal composition of 0.7 wt.% Si + Fe, 0.1 wt.% Cu, 0.05 wt.% Mn, 0.05 wt.% Mg, 0.1 wt.% Zn, 0.03 wt.% Ti, and 0.03 wt.% others and balance of Al, was provided by an industrial partner.

Prior to anodizing, as-received specimens with dimensions (6 × 4.5 × 0.105) cm were degreased by sonication in acetone for 10 minutes. Surface treatment was performed by dipping the samples in an alkaline etching solution: NaOH (40 g L^{-1}) at 40°C for 30 seconds and in a chromate-free commercial acid dismutting bath (Turco Smuttgo-Henkel) at room temperature for 15 seconds. Between each step and at the end of the surface preparation procedure, the specimens were thoroughly washed with distilled water.

Anodizing was carried out according to procedures already employed by our group by applying a constant voltage of 14 V for 20 minutes to the samples immersed in a TSA bath (40 g L^{-1} H_2SO_4 + 80 g L^{-1} $C_4H_6O_6$) maintained at 37°C.[38,39] After anodizing, the samples were rinsed with deionized water and then posttreated at a constant temperature of 50°C under different conditions: hot water for 20 minutes (HW); 50mM Ce $(NO_3)_3.6H_2O$ for 20 minutes (Ce 20M); and 50mM Ce $(NO_3)_3.6H_2O$ + 10% *v*/v H_2O_2 for 20 minutes (CeP 20M), 5 minutes (CeP 5 M), or 2 minutes (CeP 2M). Non-posttreated samples (UNS) were used as control. The experimental conditions are summarized in Table 1.

The corrosion behaviour of samples only anodized (UNS), and of samples treated with the different posttreatments was evaluated using electrochemical impedance spectroscopy (EIS) in 0.1 mol L^{-1} NaCl solution. A three-electrode cell comprising the anodized piece (12.57 cm^2 of exposed area), an Ag/AgCl reference electrode, and a platinum mesh counter electrode was employed. A potentiostat/galvanostat Solartron SI 1287 coupled to a frequency response analyser Solartron SI 1260 was used for the measurements.

TABLE 1 Posttreatment conditions

Condition	Ce $(NO_3)_3.6H_2O$, mM	H_2O_2, %	Temperature, °C	Time, min
UNS				
HW 20M			50	20
Ce 20M	50		50	20
CeP 20M	50	10	50	20
CeP 5M	50	10	50	5
CeP 2M	50	10	50	2

The frequency range was 10^5 to 10^{-1} Hz, and the amplitude of the ac signal was 15 mV with an acquisition rate of seven points per decade. Experiments were performed up to 28 days of immersion when localized corrosion spots were observed in all the surfaces of the samples. In order to verify reproducibility, measurements were performed at least in triplicate.

The morphological characterization of the samples was carried out by scanning electron microscopy (SEM) with field emission gun—FE-SEM—Inspect 50, equipped with secondary and backscattered electron detectors, and with facilities for energy dispersive X-ray analysis (EDS) (spectrometer EBSD—TEAM). Analyses were performed for uncorroded and corroded samples (after the completion of the EIS tests).

Macrograph evaluation of the surface by digital camera (Samsung ST90) was also performed after the corrosion tests.

3 | RESULTS AND DISCUSSION

3.1 | Microstructural analyses of uncorroded samples

Presented in Figure 1 are SEM micrographs showing the cross-sectional details of the Alclad AA2024-T3 sheet employed in this study. A typical clad layer with an approximate thickness of 153.5 ± 5.2 μm is revealed with far less coarse intermetallics when compared with the base metal. As reported in the literature, the clad layer galvanically protects the underlying bulk alloy[40,41] and also forms a less tortuous oxide layer during anodizing since differential oxidation resulting from the presence of coarse intermetallics rich in copper is greatly minimized.[17,38] The cross-sectional SEM image of the porous anodic layer is presented in Figure 2. The oxide thickness is in the range of (3.9 ± 0.1) μm showing that it was formed only from the consumption of a portion of the clad layer and is in accordance with others produced under similar conditions.[38] A defect is visible in the anodic oxide layer, probably associated with the presence of an intermetallic particle in the underlying clad layer.

Following anodizing, the samples were posttreated using the different procedures described in Table 1. Figure 3 depicts SEM micrographs of the surface of these samples and of a UNS sample. At the magnification at which the micrographs were obtained, significant differences between the morphologies of the surfaces of the porous layers of the samples UNS, HW, Ce 20M, CeP 5M, and CeP 2M were not observed. A scalloped surface with pores with similar and regular diameters estimated by software ImageJ (around 13.32 ± 1.58 nm) could be observed, showing that the posttreatment steps did not plug the mouths of the pores, as aimed in the present study. However, for the CeP 20M sample, the surface features were markedly different from the others. Unevenly distributed ball-shaped Ce-enriched compounds were evident all over the surface. The comparison of this surface morphology with that of the Ce 20M sample demonstrates a clear effect of the addition of hydrogen peroxide to the cerium nitrate solution. As discussed in the literature,[25] the addition of hydrogen

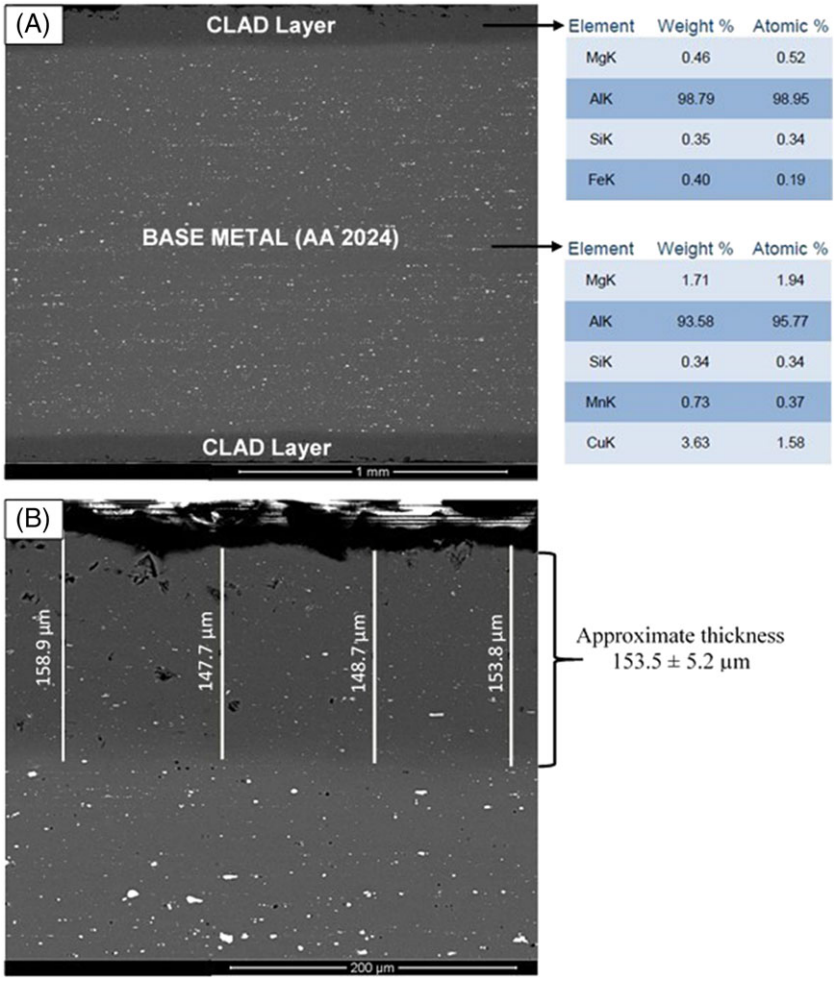

FIGURE 1 Cross-sectional SEM micrographs of the (A) Alclad AA2024-T3 alloy with EDX data obtained from the clad layer and the base metal and (B) mean thickness of the clad layer

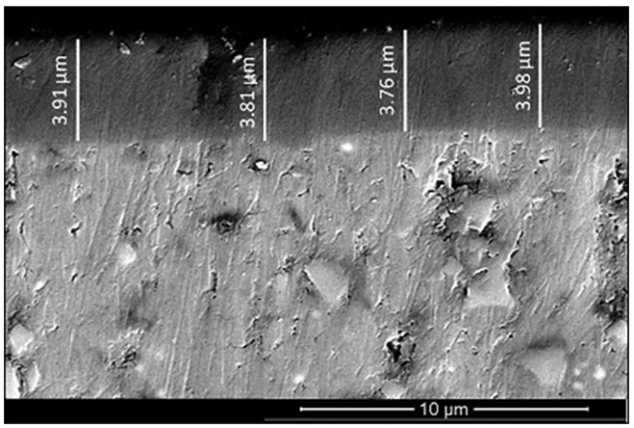

FIGURE 2 Cross-sectional SEM micrograph of the oxide layer in the TSA anodized Alclad AA2024-T3 alloy

peroxide to the posttreatment solution must accelerate the Ce (III) to Ce (IV) oxidation reaction, occurring in the bulk solution, thus increasing the deposition rate of Ce oxy-hydroxides. Moreover, the analysis of the top surface of the sample subjected to the CeP 20M posttreatment (Figure 3D) clearly shows that the anodic layer was severely etched during the posttreatment step. However, this was not the case for the CeP 2M (Figure 3F) and CeP 5M (Figure 3E) samples. These results indicate that an excessive immersion period of the anodized sample in the hydrogen peroxide-containing solution degrades the anodic oxide layer and may reduce its protective properties. Equation 1 presents the reduction reaction of H_2O_2 together with its standard potential. It shows that, besides being a powerful oxidizer, H_2O_2 reduction consumes interfacial H^+, thus increasing the local interfacial pH. Therefore, the presence of H_2O_2 would lead both to increased precipitation rate of Ce oxy-hydroxides and to chemical attack or the anodized layer, as verified in Figure 3D.[42]

$$H_2O_2(aq) + 2H^+(aq) + 2e \rightarrow 2H_2O \; E^o = +1.77V/EPH. \quad (1)$$

Figure 4 presents SEM images together with EDS analyses of some spots on the surface of CeP 2M and CeP 5M samples. They reveal that, although not forming a continuous and thick layer, Ce oxy-hydroxides deposits were sparsely formed on these samples. On the other hand, for the Ce 20M sample (without H_2O_2 addition), no evident Ce deposit could be found on the sample surface, even after a careful examination by SEM. Therefore, the addition of H_2O_2 to the posttreatment solution increases the deposition rate of Ce oxy-hydroxides, while it may lead to a chemical attack of the oxide layer upon excessive exposure, as shown in the previous paragraph.

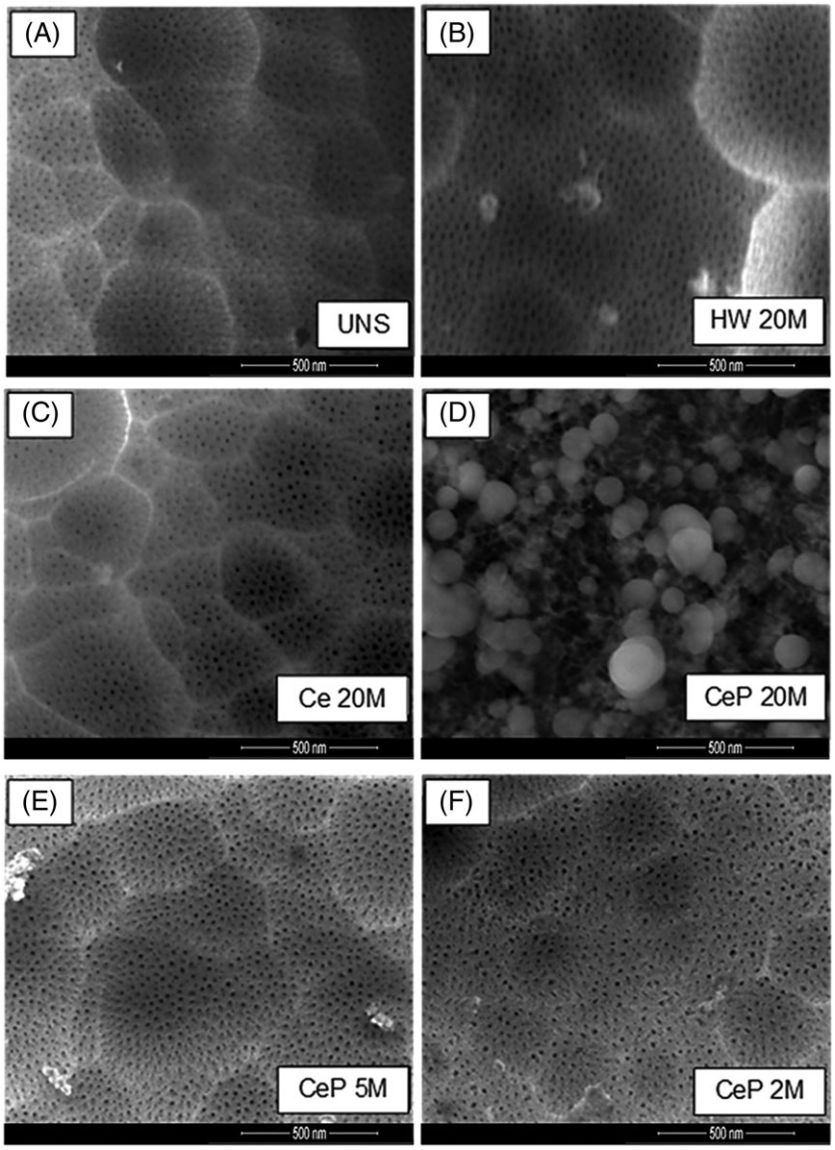

FIGURE 3 SEM micrographs of the Alclad AA2024-T3 anodized in TSA bath. (A) without (UNS) and after posttreatments, (B) HW 20M, (C) Ce 20M, (D) CeP 20M, (E) CeP 5M, (F) CeP 2M

4 | EIS MEASUREMENTS

In the literature, EIS has been widely used to investigate the corrosion process of anodized layers.[13,43] It has proved to be able to detect changes occurring throughout their thicknesses like modification of electrical properties, changes in the integrity of both the porous and barrier layer, and the effect of sealing and ageing within the pores.[44-46] These latter phenomena are of particular importance for the present investigation. Figures 5 and 6 present the EIS diagrams acquired during 672 hours (28 days) of immersion in the 0.1M NaCl solution of Alclad AA2024-T3 anodized in TSA and posttreated with the different procedures. The experiments were interrupted when visible signs of corrosion were observed on the surface of all the samples, which occurred at different degrees. Figure 5 displays the Bode plots of the UNS (reference) sample (A) and (B), together with those for samples posttreated in solutions not containing H_2O_2 (HW [C] and [D] and Ce 20M [E] and [F]), while the plots for the samples posttreated in H_2O_2 containing solutions (CeP 20M [A] and [B], CeP 5M [C] and [D], and CeP 2M [E] and [F]) are shown in Figure 6. Irrespective of the posttreatment step, the diagrams acquired after 4 and 24 hours of tests, representing the early hours of corrosion, are characterized by a single time constant spread over a wide frequency range. For these immersion times, precipitation within the pores is negligible, and the open pores are filled with the conductive electrolytic solution. Therefore, this single time constant is associated with the properties of the thin barrier layer at the bottom of the pores.[17,44] Typically, in the low frequency (LF) limit, the diagrams still exhibit a fairly capacitive response with impedance modules greater than 10^6 Ω cm^2, indicating good barrier properties of the thin oxide layer. These single time constant EIS diagrams are similar to those reported by other authors for unsealed anodized layers.

Except for the CeP 20M sample (Figure 6A,B), which keeps the one time constant response for longer test periods, for immersion times superior to 24 hours, the Bode plots of the other samples evolve to a complex two and three time constants response. These new time constants are characterized by the onset of capacitive features in the high (HF) to medium (MF) frequency domain, which are due to

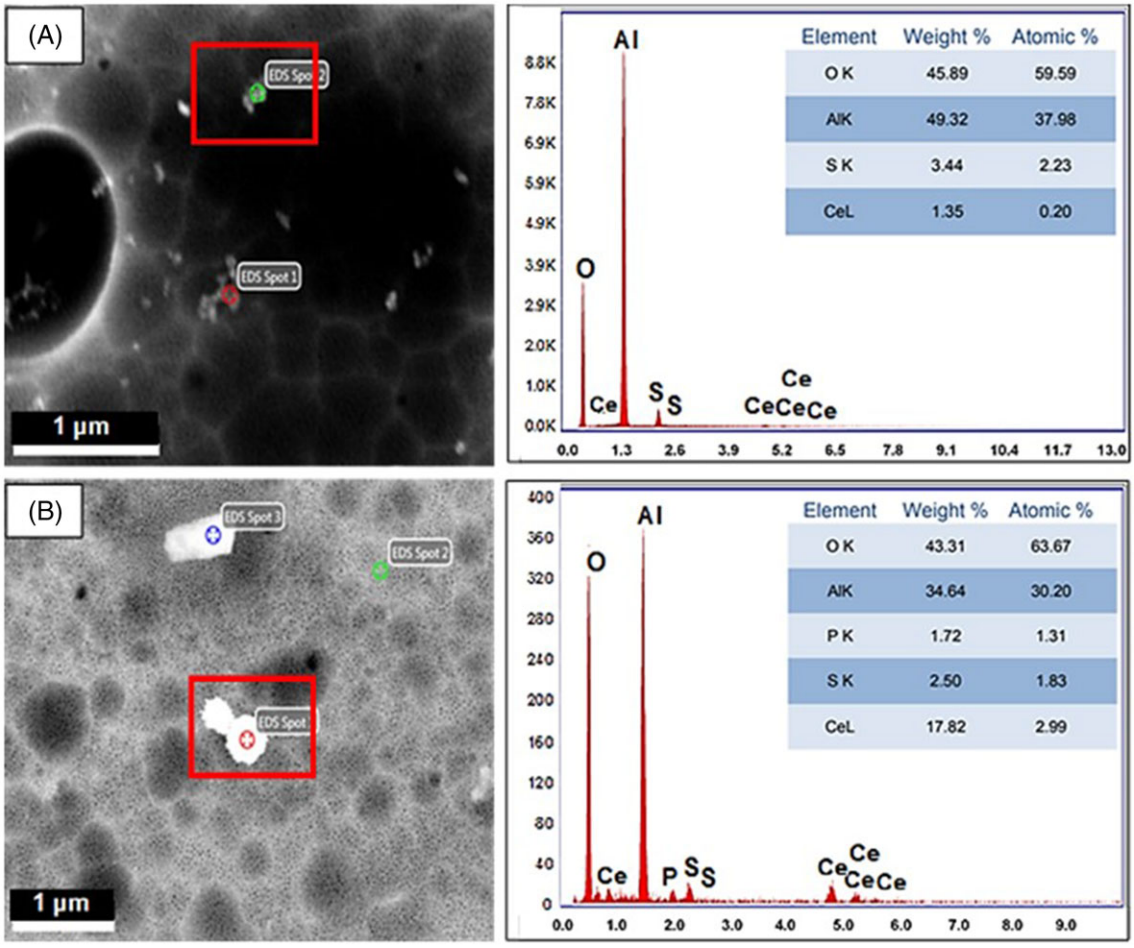

FIGURE 4 SEM-EDS micrographs of the surface of Alclad AA2024-T3 anodized in TSA and posttreated with Ce $(NO_3)_3$ + H_2O_2 for (A) 5 minutes (CeP 5M) and (b) 2 minutes (CeP 2M)

the increase of the impedance modulus in this frequency region. Several authors report two time constants response for sealed porous anodic layers, with the HF time constant being ascribed to pore sealing.[38,44,46,47] When the effect of sealing time is investigated, the better the sealing procedure the more well-defined the two time constants.[44,47] Also reported in the literature is the increase in the HF impedance modulus with sealing improvement during immersion tests.[48] Therefore, by taking the literature survey into account, the new time constants observed for exposure times longer than 24 hours can be ascribed to changes taking place within the pores. Specifically, pore blocking which, as observed in the present study, can also takes place when the porous anodic layer is exposed to the atmosphere or mildly aggressive environments.[44,48-50] It is hypothesized that, for the posttreatments involving Ce ions, these time constants may result from the precipitation of mixed Ce and Al oxy-hydroxides within the pores, with the contribution of corrosion products for longer immersion times, when three time constants are observed in the diagrams. Interestingly, even the sample with the worst corrosion resistance (CeP 20M—Figure 6A,B) exhibits an HF time constant (see diagrams obtained after 336 and 672 hours) indicating that precipitation within the pores takes place, even though not much protection seems to be afforded to the substrate for this specific sample.

Besides evident pore blocking, the diagrams of Figures 5 and 6 also show that the LF impedance modules decrease with immersion time, indicating that the precipitation (sealing) within the pores is not completely able to block the penetration of aggressive species. For most of the samples, after longer immersion periods, the LF impedance decrease is accompanied by oscillations in the phase angle. This can be associated with the onset of localized corrosion, the potential spikes characteristic of this type of corrosion leads to a nonstationary transient behaviour leading to a distortion in the impedance spectrum.[51] The extent of the LF impedance drop with immersion time was different among the samples, indicating different protective properties of the precipitated products. In order to better compare this issue, Figure 7 presents merged Nyquist plots of the six systems obtained after 336 hours (Figure 7A) and 672 hours (Figure 7B) of test in the aggressive medium, and Figure 8 depicts the variation of the LF impedance modules during the whole test period. In this latter figure, only data acquired after 24 hours are presented, as, for shorter immersion periods, a discontinuity in the LF impedance modulus with no change in the associated phase angle could be verified for all the diagrams, probably associated with the shunt resistor that is automatically selected above a certain impedance value. The plot of the LF impedance modulus has been used as a preliminary diagnosis to gauge

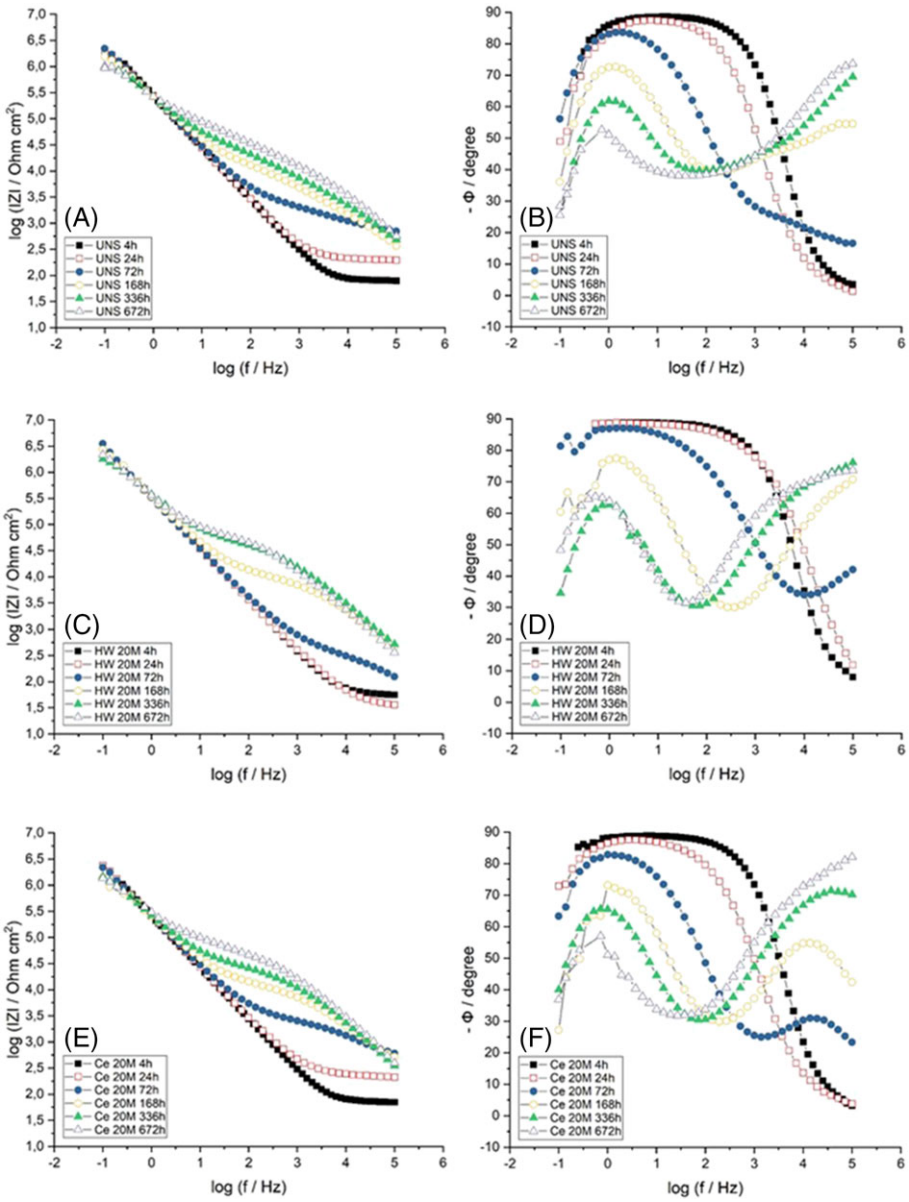

FIGURE 5 Bode plots in 0.1M NaCl solution of Alclad AA2024-T3 anodized in TSA: (A, B) untreated (UNS), and posttreated with (C, D) hot-water (HW) and (E, F) 20 minutes in 50mM Ce $(NO_3)_3$ (Ce 20M). All posttreatments were performed at 50°C

the corrosion protection afforded to metals by different protective systems.[38,52,53] Both figures show that the corrosion resistance decreases in the following order: CeP 2M > CeP 5M > HW > Ce 20M > UNS > CeP 20M, indicating that almost all the posttreatments improve the corrosion resistance of the samples when compared with the reference one. Particularly noteworthy is the stability of the LF impedance modulus of the CeP 2M sample and the fact that the samples posttreated in the H_2O_2 containing solution present the best (CeP 2M and CeP 5M) and the worst (CeP 20M) corrosion resistance. This latter response is of no surprise as it agrees well with the SEM micrographs of the posttreated surfaces earlier presented in Figure 3. The EIS results confirm that the dissolution of the alumina layer on the CeP 20M sample was excessive and probably led to the attack of the primary barrier layer. Subsequently, the deposition of the Ce-based compounds was not uniform, and as a result, the corrosion resistance offered was poor, even when compared with the UNS sample. Given that the Ce 20M sample and the CeP 20M sample were both exposed for 20 minutes at 50° C to their respective posttreatment solutions, the major difference in the response must be from the excessive exposure of the CEP 20M to the H_2O_2 containing solution, which, even though enhancing the deposition of Ce ions, attacks the oxide layer hindering the corrosion resistance.

4.1 | Equivalent circuit analysis

Four electrical equivalent circuit (EEC) models (Figure 9) were used to take into account both the complex evolution of the EIS response resulting from the changes in the porous layer morphology due to

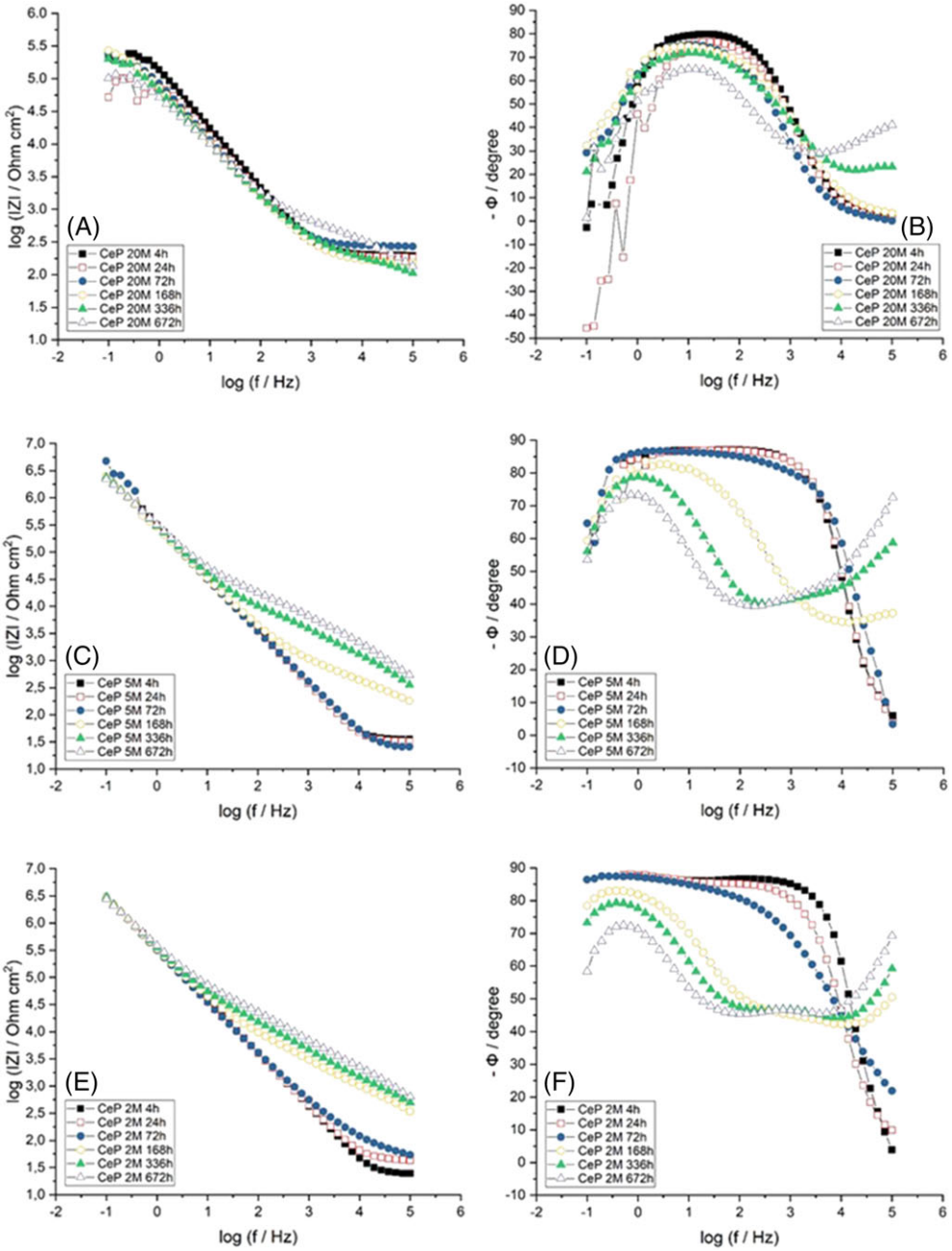

FIGURE 6 Bode plots in 0.1M NaCl solution of Alclad AA2024-T3 anodized in TSA posttreated in 50mM Ce $(NO_3)_3$ and H_2O_2 (10% vol) for (A, B) 20 minutes (CeP 20M), (C, D) 5 minutes (CeP 5M), and (E, F) 2 minutes (CeP 2M). All posttreatments were performed at 50°C

the sealing process (ageing by hydration) and the changes in the corrosion resistance while the samples were immersed in the aggressive electrolyte.[41,42] The EEC of Figure 9A was employed to fit the spectra with the single time constant, which, except for the sample CeP 20M, was verified during the early stage of corrosion (4 and 24 hours). In this EEC, Rs and Rb represent, respectively, the solution and the barrier layer resistance, and CPEb, a constant phase element (CPE) accounting for the capacitance of the barrier layer. In the EEC fitting procedure, a pure capacitive response is frequently replaced by a CPE, and the impedance is given[54] by Equation 2:

$$Z_{CPE} = \frac{1}{Q(j\omega)^n}. \quad (2)$$

In Equation 2, "n" is the dispersion factor and takes into account nonhomogeneity in the capacitive behaviour. When n = 1, the CPE is equivalent to a pure capacitor; however, when n < 1, a 2-D or 3-D distribution of properties should be expected.[55] In the former case, the CPE behaviour can be ascribed to potential and/or current distribution along the electrode surface associated with the geometry, whereas a 3-D distribution results from effects normal to the electrode surface like surface roughness and electrode porosity.[55]

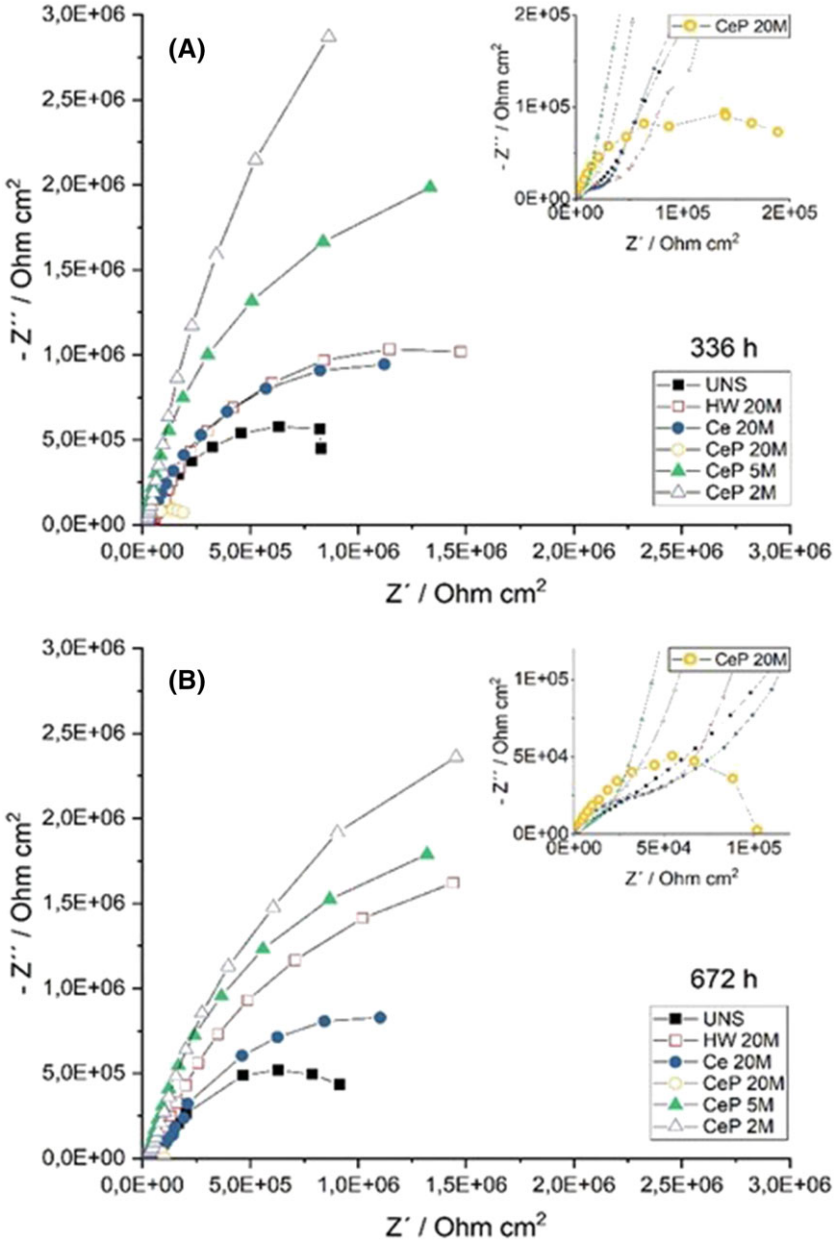

FIGURE 7 Nyquist diagrams of Alclad AA2024-T3 anodized in TSA untreated (UNS) and posttreated according to the different procedures after 336 hours (A) and 672 hours (B) of immersion in NaCl 0.1M. Zoomed diagrams evidence the lower corrosion resistance of the CeP 20M sample

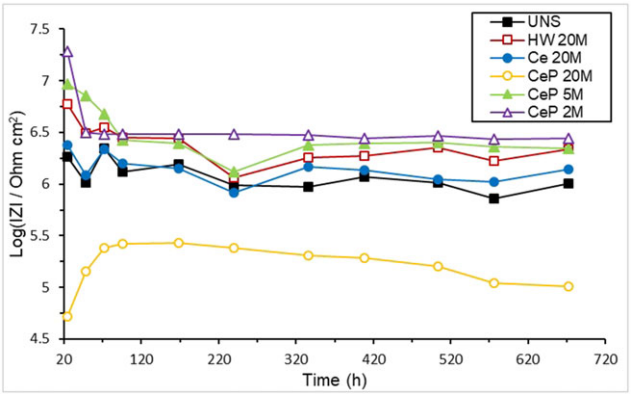

FIGURE 8 Evolution of the impedance modulus at 100 mHz with immersion time in NaCl 0.1M of Alclad AA2024-T3 anodized in TSA, untreated (UNS), and posttreated according to the different procedures. Data acquired after 24 hours of immersion

For longer immersion times, when two time constants were clearly observed in the diagrams, the EEC of Figure 9B,C were employed. The EEC of Figure 9B has been used to fit diagrams either of sealed anodized layers[45] or of unsealed layers at which precipitation occurred within the pores.[38] The added time constant (CPEp//Rp) is ascribed to the response of the precipitates within the pores. On the other hand, the EEC of Figure 9C, where a capacitance ascribed to the pore walls (Cpw) is added in parallel to the EEC of Figure 9B, is used to account for the situation when the sealing procedure is well performed, ie, when the current pathway through the precipitated products within the pores and through the barrier layer becomes more resistive.[38,39,47] Alternatively, this situation may also correspond to a condition at which an increased deterioration of the protective properties of the pore walls has taken place leading to an increase of its capacitive response due to hydration and/or thinning. However, as will be shown later by the fitting

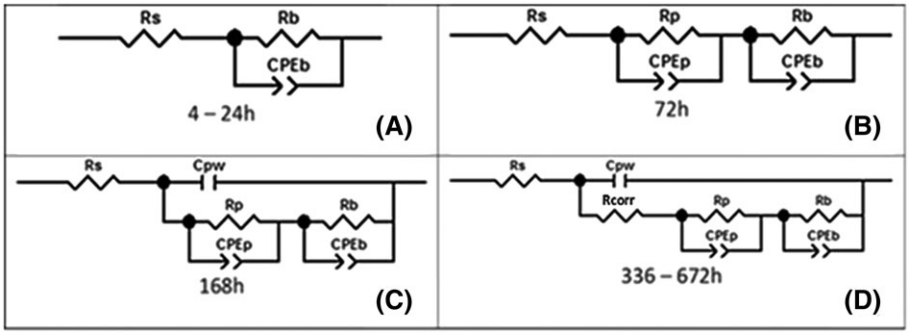

FIGURE 9 Electrical equivalent circuits (EEC) used to fit the EIS diagrams in NaCl 0.1M of Alclad AA2024-T3 anodized in TSA untreated (UNS) and posttreated according to the different procedures. Below each EEC, the immersion times at which they were most frequently used are indicated

TABLE 2 Results of the fitting procedure of the EIS diagrams with the EEC of Figure 9 for the Alclad AA2024-T3 anodized in TSA bath, without (UNS) and after posttreatments: HW 20M, Ce 20M, CeP 20M, CeP 5M, and CeP 2M

A. CPEb

Immersion Time, h	UNS CPEb ($\mu F\ cm^{-2}.S^{(n-1)}$)	UNS nb	HW 20M CPEb ($\mu F\ cm^{-2}.S^{(n-1)}$)	HW 20M nb	Ce 20M CPEb ($\mu F\ cm^{-2}.S^{(n-1)}$)	Ce 20M nb	CeP 20M CPEb ($\mu F\ cm^{-2}.S^{(n-1)}$)	CeP 20M nb	CeP 5M CPEb ($\mu F\ cm^{-2}.S^{(n-1)}$)	CeP 5M nb	CeP 2M CPEb ($\mu F\ cm^{-2}.S^{(n-1)}$)	CeP 2M nb
4	0.59	0.99	0.49	0.98	0.63	0.98	1.14	0.93	0.51	0.98	0.48	0.97
24	0.64	0.97	0.49	0.98	0.68	0.96	1.58	0.91	0.53	0.98	0.52	0.96
72	0.64	0.96	0.45	1.00	0.67	0.95	2.33	0.87	0.52	1.00	0.51	0.98
168	0.66	0.94	0.52	0.92	0.70	0.90	2.86	0.84	0.60	0.94	0.51	0.97
336	0.74	0.92	0.55	0.86	0.75	0.88	2.87	0.85	0.56	0.94	0.51	0.93
672	0.99	0.91	0.57	0.87	0.80	0.86	3.51	0.82	0.58	0.92	0.50	0.92

B. Cpw

Immersion Time, h	Cpw ($\mu F\ cm^{-2}$) UNS	HW 20M	Ce 20M	CeP 20M	CeP 5M	CeP 2M
4						
24						
72						
168	2.28E-03	2.74E-03	3.99E-03		3.98E-03	1.36E-03
336	3.09E-03	2.94E-03	4.08E-03		3.66E-03	2.80E-03
672	2.65E-03	4.09E-03	3.73E-03		3.04E-03	2.48E-03

C. CPEp

Immersion Time, h	UNS CPEp ($\mu F\ cm^{-2}.S^{(n-1)}$)	UNS np	HW 20M CPEp ($\mu F\ cm^{-2}.S^{(n-1)}$)	HW 20M np	Ce 20M CPEp ($\mu F\ cm^{-2}.S^{(n-1)}$)	Ce 20M np	CeP 20M CPEp ($\mu F\ cm^{-2}.S^{(n-1)}$)	CeP 20M np	CeP 5M CPEp ($\mu F\ cm^{-2}.S^{(n-1)}$)	CeP 5M np	CeP 2M CPEp ($\mu F\ cm^{-2}.S^{(n-1)}$)	CeP 2M np
4												
24												
72	5.02	0.51	12.28	0.50	3.12	0.49			5.48	0.85	42.22	0.53
168	2.52	0.49	1.06	0.50	1.16	0.50			8.27	0.50	7.09	0.44
336	1.78	0.49	0.25	0.59	0.70	0.51	43.49	0.50	2.83	0.51	1.70	0.56
672	1.75	0.43	0.18	0.65	0.65	0.47	11.19	0.50	1.70	0.51	1.19	0.55

results, this was not the case for the present investigation. Additionally, a parallel pore wall resistance (Rpw) also exists. However, its value is extremely high, and no conductive pathway can be developed.[56] The use of a pure capacitor to represent Cpw indicates that its property hardly changes during immersion in the aggressive electrolyte.

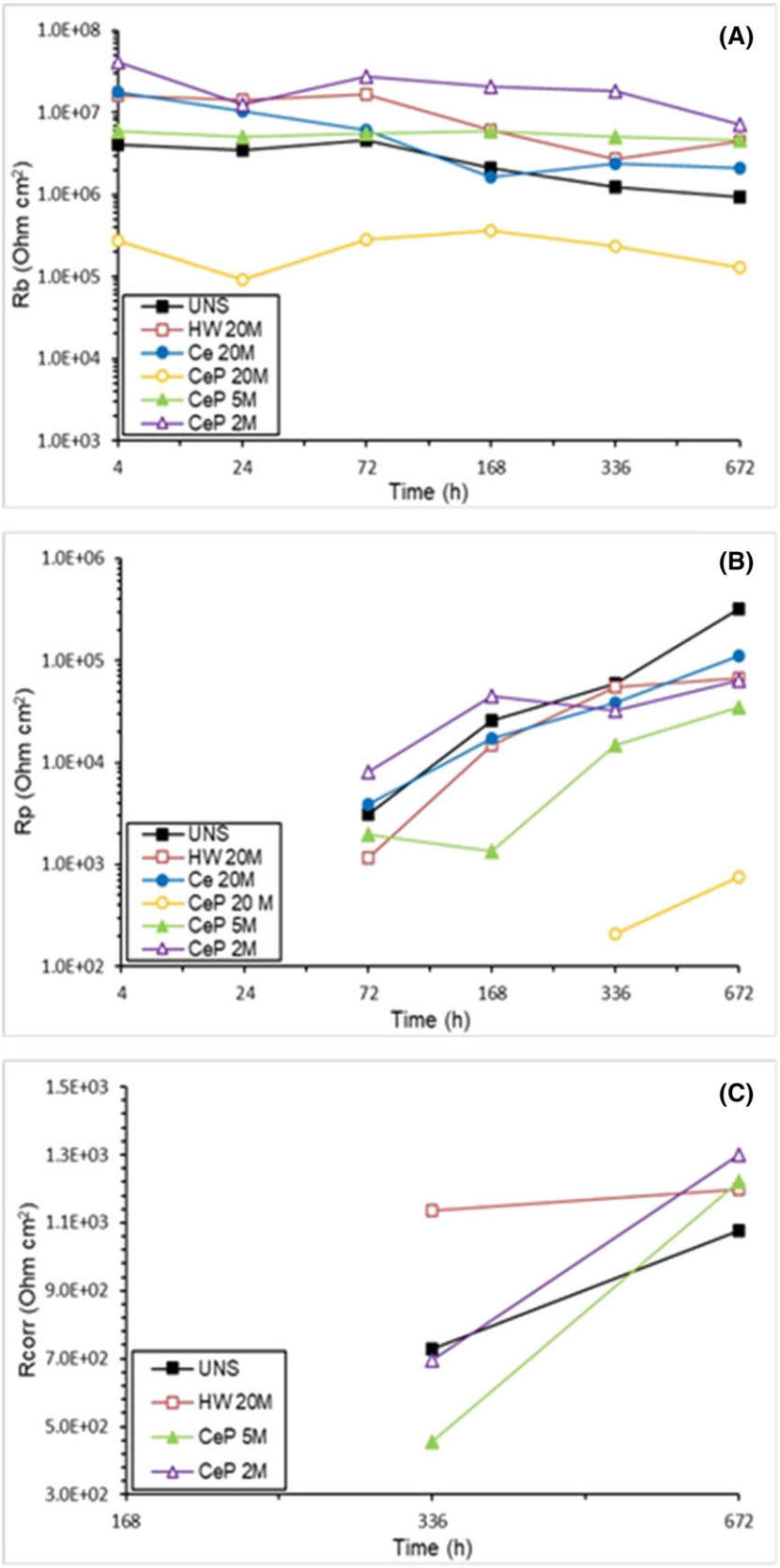

FIGURE 10 Results of the fitting procedure of the EIS diagrams with the EEC of Figure 9 for the Alclad AA2024-T3 anodized in TSA bath, without (UNS) and after posttreatments: HW 20M, Ce 20M, CeP 20M, CeP 5M, CeP 2M, (A) Rb, (B) Rp, (C) Rcorr

Finally, for longer immersion periods, when three time constants were clearly observed, the EEC of Figure 9D was employed, at which another resistive term (Rcorr) was added in parallel with Cpw and in series with the remainder of the EEC of Figure 9C. This circuit is similar to that proposed by Gonzáles et al[44] and takes into account an additional resistive pathway imposed by the precipitation of corrosion products blocking the mouths of the pores, which, nevertheless, does not hinder the penetration of aggressive species into the pores.

The results of the fitting procedures for all the treatments are presented in Table 2A to C for the capacitive elements, together with their respective "n" values, and in Figure 10A-C for the main resistive elements. The evolution of CPEb and "nb," displayed in Table 2A, shows that, whatever the sample, the values slightly increase and decrease with immersion time, respectively. Both tendencies are associated with the deterioration of the protective properties of the barrier layer, which becomes thinner/more hydrated and less homogeneous. However, the "nb" values for the samples are close to 1, especially when they are not deteriorated (short immersion periods), indicating a fairly capacitive response. Moreover, the CPEb value for the CeP 20M sample is clearly higher than for the other samples. This indicates that it is thinner, in accordance with the inferior corrosion resistance exhibited by this sample. For the other samples, the CPEb values were not very different, indicating similar properties.

The values of Cpw, presented in Table 2B, remained almost constant with immersion time, indicating that the protective properties of the porous layers were not affected by the contact with the aggressive electrolyte. The fitting of the EIS diagrams of the sample CeP 20M did not require the use of an EEC with three time constants; therefore, the EEC of Figure 9C,D were not employed to fit the diagrams of this particular sample, and no Cpw was estimated. Concerning the fitted values, they were similar for all the samples and in the order of few nF cm^{-2}, confirming its stability and high impedance. Additionally, coherent with its higher thickness, the fitted values were more than two orders of magnitude lower than those determined for CPEb.

Finally, the fitting results for CPEp, representing the properties of the products precipitated within the pores, presented in Table 2C, show "n" values close to 0.5. Classically, "n" close to 0.5 is associated with diffusion controlled processes (Warburg impedance). However, such values are frequently found in fitting procedures for sealed

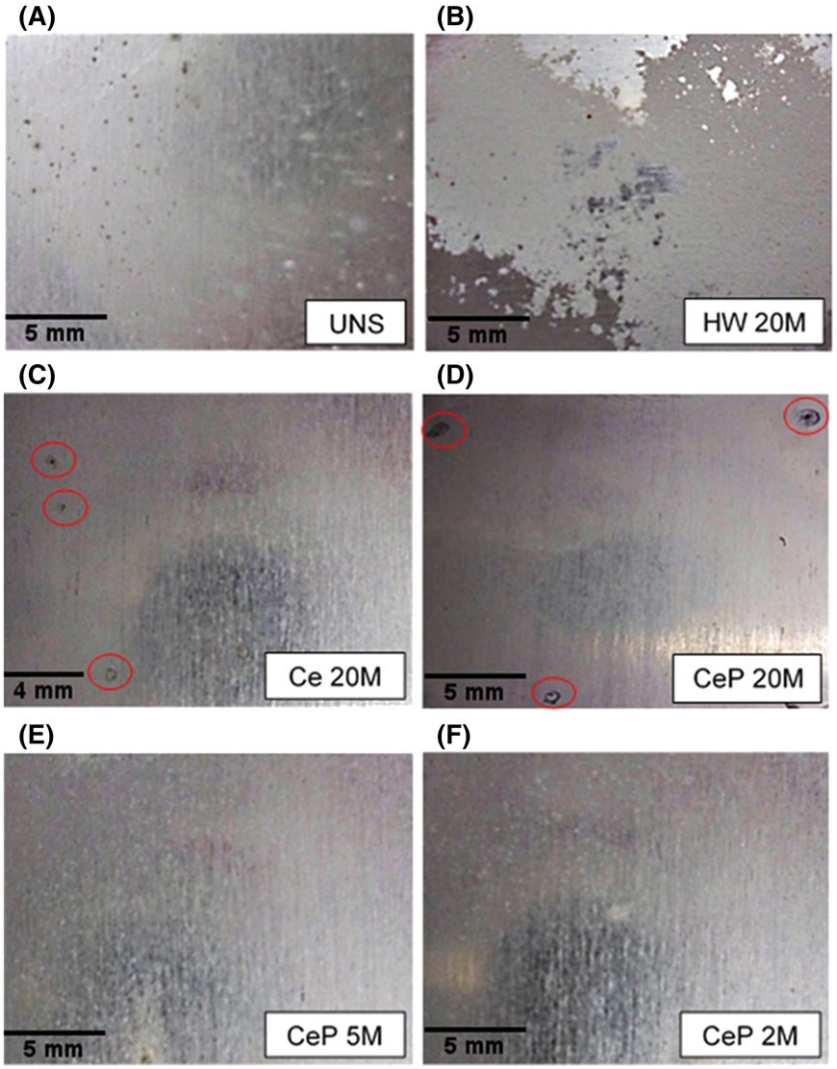

FIGURE 11 Digital images of the surfaces of the UNS (A), HW (B), Ce 20M (C), CeP 20M (D), CeP 5M (E), and CeP 2M (F) after the completion of the EIS tests; 28 days of immersion in the 0.1M NaCl

porous aluminium oxide layers.[38,39,47,48] Hoar and Wood,[56] in an article dating back to 1962, proposed that the properties of the sealed porous layer are heterogeneous and change along the pore extension. Therefore, they represented the impedance of the pores using a transmission line.[56] However, the transmission line model should be adequate to represent the EIS response of a conductive oxide layer,[57] which is not the case for the anodized aluminium oxide. Therefore, it is likely that the low "n" exponent results from a vertical distribution of time constants.[57] As the pores are only partially sealed, the current would experience different values of dielectric constants (the composition of the precipitated products should not be homogeneous) and even different geometric features along the pore extension before reaching its bottom. However, due to these facts, a direct comparison between the CPEp for the different samples would not be representative. However, the data presented in Table 2B show a decreasing trend, indicating an improvement in the sealing process.

Considering that the porous layer exhibited a pure capacitive response (Cpw) and that the exponents of CPEb were close to 1, particularly for short immersion times, the values displayed in Table 2A,B were employed to estimate, respectively, the barrier and the porous layer thicknesses (d) by means of Equation 3. Due to the similarity and stability of Cpw for all samples during the test period, an average value of 3 nF cm^{-2} was adopted. On the other hand, for the barrier layer thickness estimate, the fitting result for the unsealed sample after 4 hours immersion was adopted (5.9×10^{-7}). For the calculations, a dielectric constant (ε) of 12 was assumed for aluminium oxide (considering that ε for pure Al_2O_3 is 9.1[58] and that some hydration of both layers must occur during the anodizing procedure) and $\varepsilon^o = 8.854 \times 10^{-14}$F cm^{-1} is the vacuum permittivity.

$$d = \frac{\varepsilon\varepsilon^o}{C}. \quad (3)$$

The value calculated for the thickness of the porous layer was 3.54 μm and for the barrier layer is 18 nm. The former is in good agreement with the SEM image of Figure 2, whereas the latter lies well within the growth rate of the barrier layer, between 1.0 and 1.5 nm/V, depending on the electrolyte composition.[59,60]

Concerning the resistive elements, Rb, Rp, and Rcorr (Figure 10A-C), the two latter increase with immersion time, indicating increased precipitation within the pores and heavier corrosion product precipitation blocking the mouths of the pores, respectively, even though Rcorr was quite low, demonstrating that there is no effective blockage of aggressive species penetration. On the other hand, Rb, Figure 10A, slightly decreased, demonstrating that aggressive species can penetrate through the partially blocked pores reaching the barrier layer at their bottoms. The fitting procedure also evidenced that Rb is the main factor responsible for the good corrosion protection afforded by the anodic layer. Therefore, at the end of the exposure period, its values were about one order of magnitude higher than that of Rp, even though the latter continuously increased during the test period. Moreover, the lower corrosion resistance of the CeP 20M sample was confirmed, as the Rb values were about one order of magnitude smaller than those of the other samples. The best anticorrosion

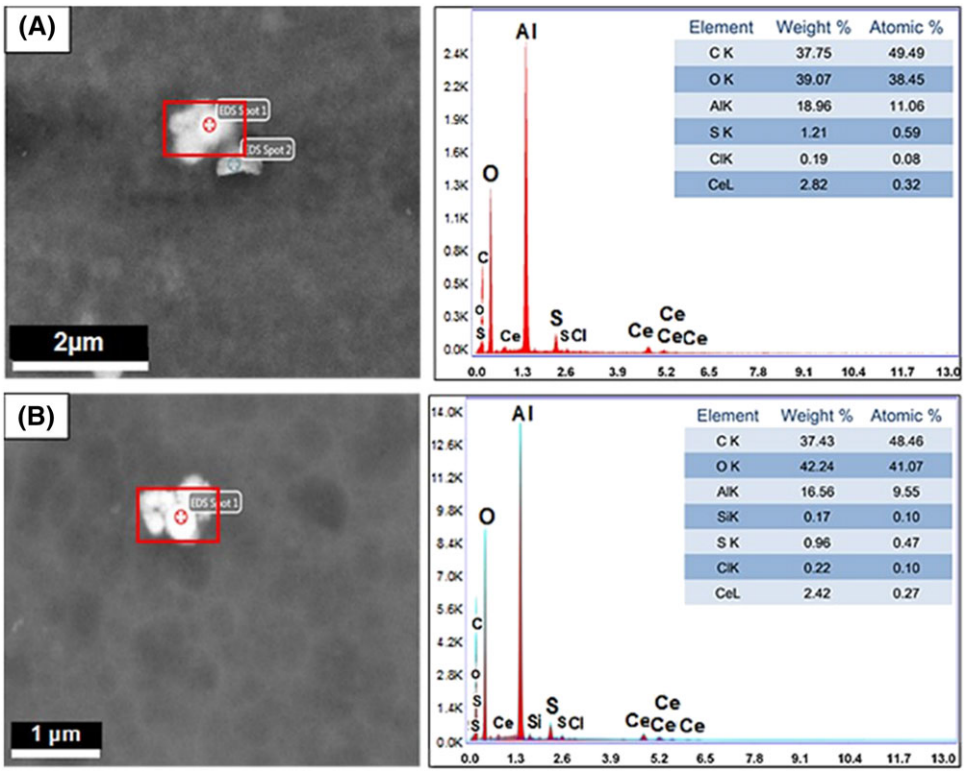

FIGURE 12 SEM micrographs and EDS analyses of precipitates on the surface of the CeP 2M (A) and CeP 5M (B) sample after 672 hours of immersion in NaCl 0.1M

performance was exhibited by the CeP 2M sample, which showed the highest and most stable Rb.

4.2 | Images of the surfaces of the samples after the EIS tests

As already stated, the EIS experiments were stopped when corrosion was visually observed at the surfaces of all samples, which intensity varied according to the posttreatment. Figure 11 depicts the digital images of the surfaces of the samples after the disassembly of the cells used in the EIS tests (672 hours of immersion). Clearly, the UNS sample (Figure 11A) exhibits the highest number of small pits, whereas the CeP 20M sample (Figure 11D) displays the biggest pits. This is in full agreement with the LF impedance modules showed in Figure 8. On the other hand, the surface of the HW sample (Figure 11B) became lustreless with evidences of general corrosion permeated with a number of medium sized pits. Ce 20M (Figure 11 D) presented a few small pits, whereas no clear differentiation could be made between samples CeP 5M (Figure 11E) and CeP 2M (Figure 11F), at which only very small pits were verified.

4.3 | SEM-EDS analysis after EIS tests in 0.1M NaCl

This research aims to incorporate Ce ions within the porous anodic layer, which, afterwards, may act as a reservoir for self-healing properties in a more complex protection system. Therefore, it is important to verify the presence of Ce oxy-hydroxides compounds on the surface of the samples after corrosion. With this purpose, SEM analyses of the surface of the samples CeP 2M and CeP 5M were performed after the completion of the EIS tests in the 0.1M NaCl solution (672 hours, corresponding to 28 days). Initially, the surface survey showed that it was no longer possible to observe the pore openings at the surface of the samples. This is in agreement with the physical structure of the anodic layer proposed for the interpretation of the EEC of Figure 9 D, wherein the pore mouths were progressively blocked by the precipitation of corrosion products. Additionally, Ce oxy-hydroxides were not found distributed all over the surface but were found randomly distributed in discrete places as globular precipitates, as highlighted in the micrographs and EDS analyses presented in Figure 12A,B, acquired, respectively, on sample CeP 2M and CeP 5M. In addition, Ce oxides were more easily found in the surface of the corroded samples when compared with the untested ones. This is a strong indication that Ce ions were stored in the microstructure of the oxide layer and may precipitate at active sites when necessary. Further work is being developed to identify the distribution, as well as the oxidation state of the Ce species at the surfaces of the samples and will be presented in future work.

5 | CONCLUSIONS

In the present work, the effect of a posttreatment step consisting of immersion in a solution at 50°C containing cerium nitrate, either without or with H_2O_2, on the corrosion resistance of Alclad AA2024-T3 anodized in TSA was investigated. The EIS results showed that the posttreatment of the anodized samples in the H_2O_2 containing bath for short immersion times (2 and 5 minutes) was the most effective in improving the corrosion resistance of the alloy. On the other hand, excessive immersion time in the same solution decreased the corrosion resistance of the anodized sample, likely due to the deterioration of the anodic layer because of pH increase. SEM surface analysis of the anodized samples after the posttreatment steps showed that the pores keep their opened structure, thus maintaining their adhesion properties, as aimed in the present investigation. However, partial pore closure was verified for the sample posttreated for longer times (20 minutes) in the H_2O_2 containing solution. SEM-EDS surface analysis of the samples posttreated in the H_2O_2 containing bath, prior and after the corrosion tests, showed the precipitation of Ce oxy-hydroxide compounds, indicating that Ce ions were incorporated in the anodic layer.

ACKNOWLEDGEMENTS

This study was supported by FAPESP Proc. 2013/13235-6 and 2018/01096-5 and CNPq Proc. 400895/2014-5 and 168625/2017-2.

ORCID

Oscar Mauricio Prada Ramirez https://orcid.org/0000-0001-6904-8959
Fernanda Martins Queiroz https://orcid.org/0000-0003-3309-1116
Uyime Donatus https://orcid.org/0000-0001-8871-3571

REFERENCES

1. Birbilis N, Buchheit RG. Electrochemical characteristics of intermetallic phases in aluminum alloys. *J Electrochem Soc*. 2005;152(4):B140-B151.
2. Thompson GE, Habazaki H, Shimizu K, et al. Anodizing of aluminium alloys. *Aircr Eng Aerosp Technol*. 1999;71(3):228-238.
3. Saenz De Miera M, Curioni M, Skeldon P, Thompson GE. The behaviour of second phase particles during anodizing of aluminium alloys. *Corros Sci*. 2010;52(7):2489-2497. https://doi.org/10.1016/j.corsci.2010.03.029.
4. Ma Y, Zhou X, Thompson GE, et al. Discontinuities in the porous anodic film formed on AA2099-T8 aluminium alloy. *Corros Sci*. 2011;53(12):4141-4151. https://doi.org/10.1016/j.corsci.2011.08.023.
5. Donatus U, Thompson GE, Zhou X. Anodizing behavior of friction stir welded dissimilar aluminum alloys. *J Electrochem Soc*. 2015;162(12):C657-C665. https://doi.org/10.1149/2.0651512jes.
6. Saenz De Miera M, Curioni M, Skeldon P, Thompson GE. Modelling the anodizing behaviour of aluminium alloys in sulphuric acid through alloy analogues. *Corros Sci*. 2008;50(12):3410-3415. https://doi.org/10.1016/j.corsci.2008.09.019.
7. Thompson GE. Porous anodic alumina: fabrication, characterization and applications. *Thin Solid Films*. 1997;297(1-2):192-201.
8. Van Den Brand J, Blajiev O, Beentjes PC, Terryn H, De Wit JH. Interaction of ester functional groups with aluminum oxide surfaces studied using infrared reflection absorption spectroscopy. *Langmuir*. 2004;20(15):6318-6326.

9. Ali N, Duan X, Jiang Z-T, et al. Surface and interface analysis of poly-hydroxyethylmethacrylate-coated anodic aluminium oxide membranes. *Appl Surf Sci*. 2014;289:560-563.
10. Lee W, Park S. Porous anodic aluminum oxide: anodization and templated synthesis of functional nanostructures. *Chem Rev*. 2014;114(15):7487-7556.
11. Abrahami ST, de Kok JM, Terryn H, Mol JMC. Towards Cr (VI)-free anodization of aluminum alloys for aerospace adhesive bonding applications: a review. *Front Chem Sci Eng*. 2017;11:1-18.
12. Kendig M, Jeanjaquet S, Addison R, Waldrop J. Role of hexavalent chromium in the inhibition of corrosion of aluminum alloys. *Surf Coat Technol*. 2001;140, p9(1):58-66.
13. Zhao X, Zuo Y, Zhao J, Xiong J, Tang Y. Study on the self-sealing process of anodic films on aluminum by EIS. *Surf Coat Technol*. 2006;200(24):6846-6853.
14. Zhao J, Xia L, Sehgal A, Lu D, McCreery RL, Frankel GS. Effects of chromate and chromate conversion coatings on corrosion of aluminum alloy 2024-T3. *Surf Coat Technol*. 2001;140(1):51-57.
15. BOEING, BAC 5632 Boric acid—sulfuric acid anodizing, Revision D, 03 ago. (2004).
16. Museux F, Theilmann R. Introducing more eco-efficient chemical treatments for aircraft structure. Towards a chromate-free Airbus. Flight air worthiness support technology (FAST), n. 45, (2009). Retrieved from: http:<//www.airbus.com/support/publications/>. Date accessed: January, 26th, 2017
17. García-Rubio M, De Lara MP, Ocón P, et al. Effect of post-treatment on the corrosion behaviour of tartaric–sulphuric anodic films. *Electrochim Acta*. 2009;54(21):4789-4800.
18. CurionI M, Skeldon P, Koroleva E, Thompson GE, Ferguson J. Role of tartaric acid on the anodizing and corrosion behavior of AA 2024 T3 aluminum alloy. *J Electrochem Soc*. 2009;156(4):C147-C153.
19. Arenas MA, Conde A, De Damborenea JJ. Effect of acid traces on hydrothermal sealing of anodising layers on 2024 aluminium alloy. *Electrochim Acta*. 2010;55(28):8704-8708.
20. Abrahami S. Cr (VI)-free pre-treatments for adhesive bonding of aerospace industry, PhD Thesis, TU Delft, 183 p., (2016).
21. Arnott DR, Ryan NE, Hinton BRW, Sexton BA, Hughes AE. Auger and XPS studies of cerium corrosion inhibition on 7075 aluminium alloy. *Appl Surf Sci*. 1985;22-23:236-251.
22. Wilson L, Hinton B. A method of forming a corrosion resistant coating, Australian Patent WO 88/06639 (1988).
23. Hinton BRW. Corrosion inhibition with rare earth metal salts. *J Alloys Compd*. 1992;180(1-2):15-25.
24. Hughes AE, Scholes FH, Glenn AM, Lau D, Muster TH, Hardin SG. Factors influencing the deposition of Ce-based conversion coatings, part I: the role of Al3+ ions. *Surf Coat Technol*. 2009;203(19):2927-2936.
25. Lau D, Glenn AM, Hughes AE, Scholes FH, Muster TH, Hardin SG. Factors influencing the deposition of Ce-based conversion coatings, part II: the role of localised reactions. *Surf Coat Technol*. 2009;203(19):2937-2945.
26. Dabalà M, Armelao L, Buchberger A, Calliari I. Ce-based conversion layers on aluminum alloys; J H W de W P Campestrini, H Terryn, A. Hovestad, "Formation of a cerium-based conversion coating on AA2024: relationship with the microstructure,". *Surf Coat Technol*. 2003;176:365-381.
27. Palomino LEM, De Castro JFW, Aoki IV, De Melo HG. Microstructural and electrochemical characterization of environmentally friendly conversion layers on aluminium alloys. *J Braz Chem Soc*. 2003;14(4):651-659.
28. Palomino LM, Suegama PH, Aoki IV, Montemor MF, De Melo HG. Electrochemical study of modified cerium–silane bi-layer on Al alloy 2024-T3. *Corros Sci*. 2009;51(6):1238-1250.
29. Ershov S, Druart M-E, Poelman M, Cossement D, Snyders R, Olivier M-G. Deposition of cerium oxide thin films by reactive magnetron sputtering for the development of corrosion protective coatings. *Corros Sci*. 2013;75:158-168.
30. Yoganandan G, Pradeep Premkumar K, Balaraju JN. Evaluation of corrosion resistance and self-healing behavior of zirconium–cerium conversion coating developed on AA2024 alloy. *Surf Coat Technol*. 2015;270:249-258.
31. Snihirova D, Lamaka SV, Montemor MF. "SMART" protective ability of water based epoxy coatings loaded with CaCO3 microbeads impregnated with corrosion inhibitors applied on AA2024 substrates. *Electrochim Acta*. 2012;83:439-447.
32. Carneiro J, Tedim J, Fernandes SCM, et al. Chitosan-based self-healing protective coatings doped with cerium nitrate for corrosion protection of aluminum alloy 2024. *Prog Org Coat*. 2012;75(1-2):8-13.
33. Jegdic BV, Zivkovic LJS, Popic JP, Rogan J, Bajat JB, Miskovic-Stankovic VB. Corrosion stability of cerium-doped cataphoretic epoxy coatings on AA6060 alloy. *Mater Corros*. 2016;67(11):1173-1184.
34. Hu T, Shi H, Fan S, Liu F, Han E-H. Cerium tartrate as a pigment in epoxy coatings for corrosion protection of AA 2024-T3. *Prog Org Coat*. 2017;105:123-131.
35. Carangelo A, Curioni M, Acquesta A, Monetta T, Bellucci F. Cerium-based sealing of anodic films on AA2024T3: effect of pore morphology on anticorrosion performance. *J Electrochem Soc*. 2016;163(14):C907-C916.
36. Gordovskaya IV, Hashimoto T, Walton J, Curioni M, Thompson GE, Skeldon P. Development of cerium-rich layers on anodic films formed on pure aluminium and AA7075 T6 alloy. *J Electrochem Soc*. 2014;161(14):C601-C606.
37. Carangelo A, Curioni M, Acquesta A, Monetta T, Bellucci F. Application of EIS to in situ characterization of hydrothermal sealing of anodized aluminum alloys: comparison between hexavalent chromium-based sealing, hot water sealing and cerium-based sealing. *J Electrochem Soc*. 2016;163(10):C619-C626.
38. Capelossi VR, Poelman M, Recloux I, Hernandez RPB, De Melo HG, Olivier MG. Corrosion protection of clad 2024 aluminum alloy anodized in tartaric-sulfuric acid bath and protected with hybrid sol-gel coating. *Electrochim Acta*. 2014;124:69-79.
39. Costenaro H, Queiroz FM, Terada M, Olivier MG, Costa I, De Melo HG. Corrosion protection of AA2524-T3 anodized in tartaric-sulfuric acid bath and protected with hybrid sol-gel coating. *Key Eng Mater*. 2016;710:210-215.
40. DAVIS AND ASSOCIATES. Aluminum and aluminum alloys. In: Davies JR, ed. *ASM Specialty Handbook*. Geauga County: ASM International; 1993.
41. Petroyiannis PV, Pantelakis SG, Haidemenopoulos GN. Protective role of local Al cladding against corrosion damage and hydrogen embrittlement of 2024 aluminum alloy specimens. *Theor Appl Fract Mech*. 2005;44(1):70-81.
42. Campestrini P, Terryn H, Hovestad A, De Wit JHW. Formation of a cerium- based conversion coating on AA2024: relationship with the microstructure. *Surf Coat Technol*. 2004;176(3):365-381.
43. Domingues L, Fernandes JCS, Da Cunha Belo M, Ferreira MGS, Guerra-Rosa L. Anodising of Al 2024-T3 in a modified sulphuric acid/boric acid bath for aeronautical applications. *Corros Sci*. 2003;45(1):149-160.

44. González JA, Lopez V, Bautista A, Otero E. Characterization of porous aluminium oxide films from a.c. impedance measurements. *J Appl Electrochem*. 1999;29(2):229-238.
45. Hitzig J, Jüttner K, Lorenz WJ, Paatsch W. AC-Impedance measurements on corroded porous aluminum oxide films. *J Electrochem Soc*. 1986;133(5):887-892.
46. Hitzig J, Juttner K, Lorenz WJ, Paatsch W. Ac-impedance measurements on porous aluminium oxide films. *Corros Sci*. 1984;24, b(11/12):945-952.
47. Boisier G, Pébère N, Druez C, Villatte M, Suel S. FESEM and EIS study of sealed AA2024 T3 anodized in sulfuric acid electrolytes: influence of tartaric acid. *J Electrochem Soc*. 2008;155(11):C521-C529.
48. Yang J, Yang Y, Balaskas A, Curioni M. Development of a chromium-free post-anodizing treatment based on 2-mercaptobenzothiazole for corrosion protection of AA2024T3. *J Electrochem Soc*. 2017;164(7):C376-C382.
49. Hao L, Cheng BR. Sealing processes of anodic coatings-past, present and future. *Met Finish*. 2000;98(12):8-18.
50. López V, Bartolomé MJ, Escudero E, Otero E, González JA. Comparison by SEM, TEM, and EIS of hydrothermally sealed and cold sealed aluminum anodic oxides. *J Electrochem Soc*. 2006;153(3):B75-B82.
51. Van Gheem E, Pintelon R, Vereecken J, et al. Electrochemical impedance spectroscopy in the presence of non-linear distortions and non-stationary behaviour: part I: theory and validation. *Electrochim Acta*. 2004;49(26):4753-4762.
52. Bravo-Anagua E, Aoki IV. Influence of cerium ions and shelf-life of hybrid solution as pretreatment for AA 2024 aluminum alloy on its anticorrosion performance. *Surf Interface Anal*. 2016;48(8):809-817.
53. Costenaro H, Lanzutti A, Paint Y, et al. Corrosion resistance of 2524 Al alloy anodized in tartaric-sulphuric acid at different voltages and protected with a TEOS-GPTMS hybrid sol-gel coating. *Surf Coat Technol*. 2017;324:438-450.
54. Barsoukov E, Macdonald J. In: Barsoukov E, Macdonald J, eds. *Impedance Spectroscopy: Theory, Experiment, and Applications*. 2nd ed. New Jersey: John Wiley and Sons; 2005.
55. Jorcin J-B, Orazem ME, Pébère N, Tribollet B. CPE analysis by local electrochemical impedance spectroscopy. *Electrochim Acta*. 2006;51(8-9):1473-1479.
56. Hoar TP, Wood GC. The sealing of porous anodic oxide films on aluminium. *Electrochim Acta*. 1962;7(3):333-353.
57. Orazem M, Tribollet B. *Electrochemical Impedance Spectroscopy*. 2nd ed. Hoboken, New Jersey: John Wiley & Sons, Inc.; 2017:768.
58. Glückert JT. Optical Spectroscopy of Individual Single-Walled Carbon Nanotubes in an Electric Gate Structure: Tuning the Photoluminescence with Electric Fields, Dissertation of the Faculty of Physics of the Ludwig-Maximilians-University Munich, 161 p, (2014).
59. Brevnov DA, Rao GVR, López GP, Atanassov PB. Dynamics and temperature dependence of etching processes of porous and barrier aluminum oxide layers. *Electrochim Acta*. 2004;49(15):2487-2494.
60. Patermarakis G, Plytas J. A novel theory interpreting the extremes of current during potentiostatic anodising of Al and the mechanisms of normal and abnormal growth of porous anodic alumina films. *J Electroanal Chem*. 2016;769:97-117.

How to cite this article: Prada Ramirez OM, Queiroz FM, Terada M, et al. EIS investigation of a Ce-based posttreatment step on the corrosion behaviour of Alclad AA2024 anodized in TSA. *Surf Interface Anal*. 2019;51:1260–1275. https://doi.org/10.1002/sia.6633